Relevant Material for Lecture 11

"Galaxies: Structure, Dynamics, and Evolution"

8 Evolution with redshift

In the last handout we discussed how the nearby universe looked like. What can we say about evolution ? We can do a simple thing: try to model the nearby galaxies, determine their past star formation histories, and stick to those models. However, this is not very pleasing: the models may clearly be wrong.
Hence, we can turn the problem around: we can look at galaxies in the distant universe, determine their star formation rates and masses, and see how the universe at high redshift compares to the universe in the nearby universe.
A major practical problem occurs: a vast amount of telescope time is needed to get spectra and redshifts of galaxies. Why ? SDSS looked at galaxies brighter than 17.8 in the r band, and nearly 1e6 of them. However, typical galaxies at $z = 1$ have r band magnitudes fainter by 5 or more magnitudes - requiring 1e4 longer integration times to get the same signal-to-noise.
With larger telescopes one can gain a factor of 16 in area - but it is easy to see that this is not enough to do surveys as large as the SDSS at high redshift.

There are two solutions:

- do surveys on smaller areas and smaller numbers
- try to estimate the redshifts from (narrowband) photometry, not spectroscopy

Both approaches are being used a lot these days

Both types of surveys start with wide-field imaging to find the galaxies.
It is generally best to image the fields with as many bands as possible.

For example:
U, B, V, R, I, z in the optical
J, H, K in the near-IR
3.6, 4.5, 5.8, 8 μ m with IRAC on Spitzer 24μm, 70 μm, 160 μm with MIPS on Spitzer

plus radio, Xray, UV from GALEX, etc..

Not all of these bands are necessary - some specific studies use many fewer bands.

Studies to z=1.5

Studies to $z = 1.5$ are usually based on imaging in the optical. Galaxies are generally selected in a red band, so that the selection band lies redward of the 4000 Å break (or close to it). The light redward of the 4000 Å break correlates better with stellar mass than the light blueward of it.

Then, large numbers spectra are taken (e.g., DEEP 2 survey, Davis et al 2003, Faber et al. 2007). This survey used the Keck telescope, to take 11.000 spectra out to $z = 1.4$. Galaxies were selected in the R band. The area was 3.5 deg^2. To avoid too many galaxies at low redshift, a color selection was used.
A special spectrograph was used to take the spectra. It is called DEIMOS, and it is a giant !

The DEIMOS spectrograph under construction in the UCO/Lick Observatory Instrument Laboratory.

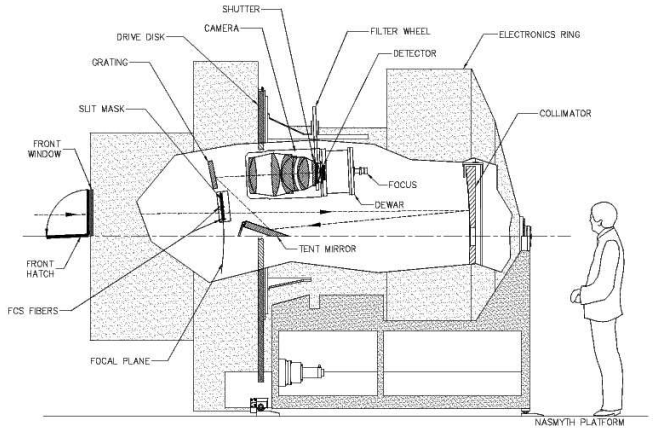

Figure 2. Light path and major optical components.

The largest element is about 1m - the size of a small telescope.

The instrument can take more than 100 spectra at high spectral resolution. The latter is important, as the night sky is full with emission lines in the red ($\lambda >$ 6000 Å). Only with high resolution can one look "between" the emission lines.

With a slit mask with many short slits, one can take many spectra. The output is shown below:

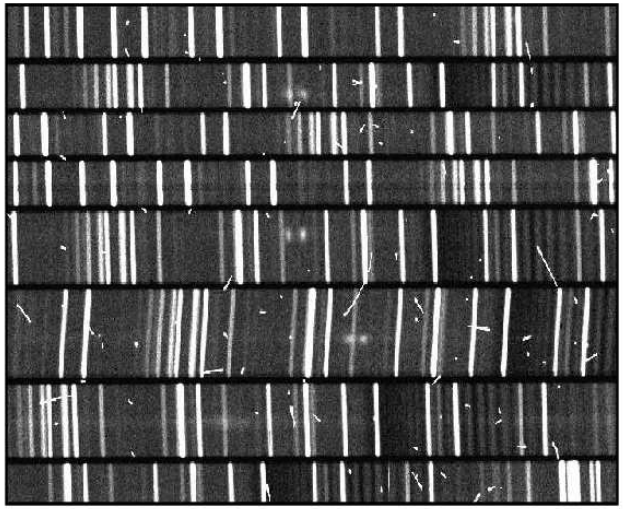

Figure 4. A 700 by 300 pixel section of the coadded raw frames of one mask, with total integration time of one hour. The tilted sky lines indicate the tilt of the individual slitlets. Cosmic rays are prominent, but note as well the sets of double emission lines in the spectra.

This is a raw image from the spectrograph. You can see the individual spectra, and the skylines. The skylines are much brigher than the galaxies. Even the continuum sky is quite bright. Furthermore, lots of cosmic rays can be seen. Some of the slits are tilted, because the mask was designed with tilted slits, to lie along the major axis of the galaxies (for some, not all)

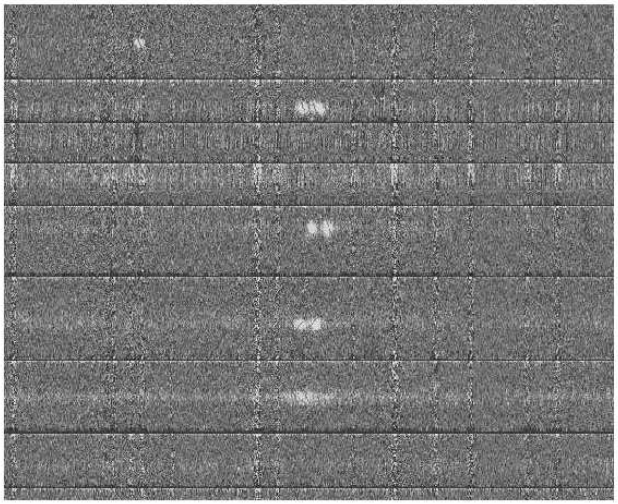

Figure 5. A same small piece of a single mask shown in figure 4, now having passed through the reduction pipeline. The spectra are now aligned in wavelength, and the noisy vertical lines are residuals of the OH forest after sky subtraction. The plot does not capture the fact that these lines have mean zero and noise consistent with their Poisson fluctuation. The double emission lines on the four objects in the middle of the plot are [OII] 3727 $\AA$ lines at $z \sim 1$ (the split of the doublet is 220 km/s). This is a modest group of galaxies, one of the thousand or so expected within the DEEP2 Redshift Survey.

These are the spectra after careful skysubtraction. We can now see the emission lines very clearly - but it is also clear that the continuum is not very visible - that requires much longer integration times.

The goals of the survey are listed on the next page (Davis et al 2003)

Goal 1: Determine the characteristics of galaxies at $z \sim 1$ and their dependence on environment; e.g. measure the evolution of the "structure function" of galaxies with redshift. DEEP2 will measure a wide variety of parameters of the observed galaxies: not just colors, magnitudes, and redshifts, but also in many cases linewidths or rotation velocities, equivalent widths of emission lines (and thereby such parameters as metallicity and O[II]-derived star formation rates), the ages of stellar populations, etc., etc. The distributions of and correlations between these parameters, along with their evolution to the present epoch, will provide strong constraints on models of galaxy formation and evolution, whether semi-analytic (e.g. Refs. 6, 7) or based on N-body simulations (e.g. Refs. 8, 9). An example of this sort of DEEP2 science which is critically dependent on combining ground-based spectroscopy with space-based imaging is the measurement of the "structure function" of galaxies.

In general a set of two parameters, such as a scale radius and internal velocity, are sufficient to characterize the structure of a typical dark matter halo.[10,11] Current theories for galaxy formation predict different evolving relationships between these dark halo parameters and observable galaxy properties such as luminosities (e.g. Refs. 7, 12. The "structure function" is a compact way of characterizing these relationships at any epoch. Each galaxy can be represented by its radius, luminosity, and internal velocity—a point in so-called "Fundamental Plane" space. The co-moving number density of galaxies in this space is what we term the "structure function," by analogy with the familiar luminosity function. A 1-d projection of the structure function onto the luminosity axis generates the luminosity function, while 2-d projections onto planes generate the Tully-Fisher and D_n-σ functions. A major goal of DEEP2 is to measure the full structure function at $z \sim 1$ in a wide variety of environments (from near-voids to clusters) and compare it to today's. DEEP2 will measure two parts of this function well: internal velocities of galaxies can be measured spectroscopically down to ~ 25 km s^{-1}(limited by the resolution of our spectra); while the ground-based BRI imaging can be used to measure the (rest-frame B) luminosities of the target objects. However, from the ground we can derive radii only for the largest, most spatially extended (or relatively nearby) galaxies.

Thus, measurement of the full structure function will only be possible with the addition of high-resolution space-based images (adaptive optics from the ground is still limited to comparatively tiny fields of view). The ACS instrument recently installed on HST is ideal for this task. With measurements of radii from HST, the 3HS would provide complete structural data for about 5,000 galaxies, sufficient to allow subdivision by galaxy type and environment; the 1HS objects in the same fields would provide $\sim 5,000$ more. Most galaxies of the 1HS will lack accurate radii (unless HST imaging were eventually obtained for all the DEEP2 fields) but will still provide excellent data on the luminosity function, $N(L)$, the velocity function, $N(v)$, and the Tully-Fisher function, $N(L, v)$. If the cosmic input parameters (Ω_m, Ω_Λ, etc.) are known from other measurements, these functions $N(L)$, $N(v)$, and $N(L, v)$ will also provide useful tests of the baryonic infall physics of galaxies.

In addition, Palomar K-band imaging will be performed over the full 1HS survey region, which will provide invaluable information on stellar masses for galaxies at $Z \sim 1$. The K-band photometry, combined with linewidths and HST determined sizes, will also allow us to determine stellar to total mass ratios. This is an important quantity, but has hardly been attempted at high redshift; DEEP2 should be able to do it for many galaxies.

Goal 2: Measure the two-point and higher-order correlation functions of galaxies at $z \sim 1$ as a function of other observables. In almost all models of structure formation (e.g., Ref. 13), galaxies are born as highly biased tracers of the mass distribution, but their bias diminishes with time. Spiral galaxies today appear to be weakly biased, if at all, while the clustering of $z \sim 3$ Lyman-break galaxies requires a large bias for any reasonable cosmological model.[14,15] Galaxies at $z \sim 1$ should have an intermediate degree of bias, with readily observable consequences. With sufficiently dense sampling, determining the higher-order clustering properties of galaxies can yield direct measurements of their biasing.[16,17] It will be possible to subdivide the 1HS sample as a function of galaxy type, luminosity, etc. and measure the biasing for each sample both in an absolute sense and compared to the other samples. This and other, more sophisticated measures will be explored as part of DEEP2. The 1HS survey is designed to provide a fair sample volume for analysis of LSS statistical behavior, particularly for clustering studies on scales $< 10h^{-1}$ Mpc. The comoving volume surveyed in the 1HS program will exceed that of the LCRS survey,[4] a survey which has proven to be an outstanding resource for low redshift studies of LSS.

Goal 3: Determine the evolution of the abundance of dark matter halos and clusters as a function of internal velocity, $N(v, z)$. By measuring the linewidths of parent dark matter halos from the galaxies visible within them (as per Goal 1 above), we can use the dark-halo abundance as a function of internal velocity and redshift, $N(v, z)$, to perform a classic cosmological test. It is well known that the volume element $dV/dzd\omega$ (where ω is solid angle) strongly depends on the input cosmological parameters, notably Ω_m and Ω_Λ. Thus, the apparent number of objects with a given linewidth versus redshift is a sensitive test of the volume element—provided the co-moving number density of those objects is known. In practice, the poorly-known evolution of the number density $N(L)$ of galaxies has stymied this test. However, if we have measured real potential-well depths, we can bypass galaxies and count the more easily simulated dark halos directly. This work will require us to study a significant fraction of our galaxies with the high resolution of HST to ensure that these objects are morphologically simple, and thus that their linewidths provide real information about the potential wells of galaxies. Newman & Davis[19,20] showed that the degree of evolution in the comoving number density of galaxy sized halos at fixed velocity is almost totally independent of cosmology. The observed abundance of such objects, $dN(v)/dz$, thus measures the volume element of the expanding Universe and gives us a powerful handle on the cosmic geometry.

In contrast, the time evolution of the comoving number density of groups and clusters of galaxies is exponentially sensitive to certain combinations of cosmological parameters – much stronger than the differences in volume amongst models. Thus, the detected abundance of clusters provides a separate, very powerful probe of the cosmological parameters (e.g. Ref. 18). Based on tests with mock catalogs from simulations, we expect to measure the abundance of clusters as a function of their velocity dispersion – which can be predicted directly from models of the dark matter distribution – down to a dispersion of ~ 400 km s^{-1}at $z \sim 1$.[21,22] This provides another test of the cosmology, complementary to the one provided by counts of galaxies.

Both techniques can place constraints not only on spatially curved models containing matter and possibly a simple cosmological constant, but also on flat "quintessence" models in which the dark energy is assumed to consist of an active field with an effective equation of state $P = w\rho$, with $-1 < w < -1/3$ ($w = -1$ for a cosmological constant; cf. Ref. 26). The equation of state parameter w can only be measured via global cosmological tests; prospects for constraining it from CMB analyses alone are relatively poor.[23]

Goal 4: Measure redshift-space distortions due to peculiar velocities at $z \sim 1$. The clustering of galaxies is inherently isotropic in space, with no preferred orientation toward or away from the Milky Way. The observed redshift-space clustering of galaxies, however, is distorted by peculiar velocities, producing features such as the so-called "fingers of God" on virialized scales and a flattening of structure on larger scales. DEIMOS will deliver highly precise redshifts, allowing both of these effects to be readily detectable in our maps (see Ref. 24 for details).

A variety of statistical tools have been developed to extract pair- and object-weighted velocity dispersions as well as measures of the flattening on larger, non-virialized scales. Analysis of these quantities will give us strong measures of a degenerate combination of Ω_m at $z \sim 1$ and the bias of the galaxy distribution. This degeneracy can be broken by comparison to the same statistics at $z \sim 0$. By these analyses we can get a strong handle on the bias of the galaxy distribution and can study the success and failures of our paradigm of structure formation. With DEEP2 we can construct at $z \sim 1$ the detailed statistics of velocity fields that have only recently been possible at $z \sim 0$[25] !.

5. DATA FLOW FOR THE DEEP2 REDSHIFT SURVEY

The data rate from DEIMOS will be in excess of 1 Gbyte/hour, necessitating automated reduction and analysis tools. We have therefore developed a spectral reduction pipeline for DEIMOS based upon the remarkable pipeline developed by D. Schlegel and S. Burles for the SDSS spectroscopic survey. We are extremely indebted to them for allowing us to study their code and extract its core elements. As shown above, we are routinely achieving Poisson limited sky subtraction even amidst the OH forest, which is made possible by careful attention to the 2-d wavelength solution within each slitlet and by the use of b-splines for a precision fit of the sky spectrum within each slitlet. Details of this spectral reduction pipeline will be provided elsewhere.

Basic results

The most basic result coming out of the survey is the evolution of the density of red and blue galaxies with redshift. The next figure shows the color distribution of the galaxies as a function of redshift.

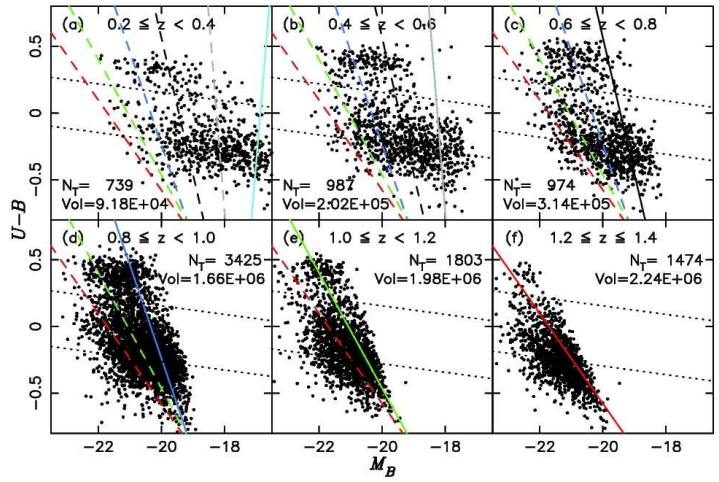

FIG. 4.—Rest-frame CM diagrams for DEEP2 for the redshift intervals used in this work. The three lower z intervals (*a*, *b*, and *c*) contain only EGS data, while galaxies in all four DEEP2 fields are shown for $z \geq 0.8$. The solid line in each panel indicates the approximate faint absolute magnitude limit as a function of intrinsic color and redshift for a sample with a fixed apparent magnitude limit $R_{\rm vega} = 23.88$. This line is calculated at the *upper* redshift limit of each panel and denotes the limiting magnitude for which a volume-limited sample could be defined in that bin. This calculation uses the distance modulus and the K-correction appropriate for each template SED, which is then fit by a linear relation, corresponding to the plotted line. The dashed lines repeat the same lines in other panels. The upper dotted line denotes the cut used to define red-sequence galaxies (eq. [19]) and is the same at all redshifts. The lower dotted line is drawn parallel to this, but its vertical height is displaced downward in each redshift bin to divide very blue from moderately blue galaxies into two equal halves (see § 4.2). The numbers in each panel show the number of galaxies plotted and the comoving volume in Mpc^3 for the $(H_0, \Omega, \Lambda) = (70, 0.3, 0.7)$ cosmology.

One can clearly see the red sequence out to $z = 1$. This is expected - $z = 1$ is only 6 Gyr ago - and people think that ellipticals are much older than that.

This result was obtained earlier by Bell et al 2004 - not by taking spectroscopic redshifts, but by photometric redshifts. This method works in the following way. Take spectra at low resolution - through 17 filters

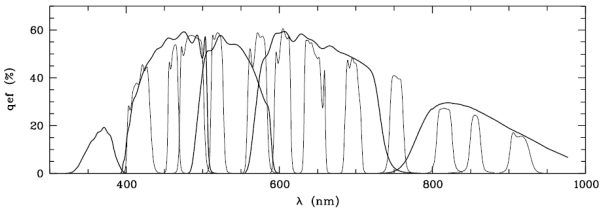

Fig. 1. COMBO-17 filter set: total system efficiencies in the COMBO-17 bands. They include two telescope mirrors, the WFI instrument, CCD detector and an average La Silla atmosphere. Photometric calibrations of such datasets are best achieved with spectrophotometric standards inside the target field.

One can derive fairly accurate photometric redshifts this way. See:

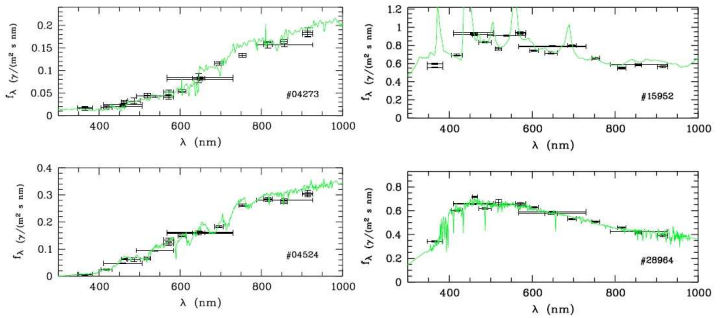

Fig. 3. *Medium-band power*: pair comparison between objects with similar *BVRI* colours, where different medium-band SEDs break the degeneracies in broad-band colour diagrams. Multiple error bars mean multiple observations at different epochs. *Left panels*: a $z = 0.67$ galaxy with modest star formation (*top*) and an M1 star (*bottom*). *Right panels*: a $z = 2.6$ quasar (*top*) and an F2 star (*bottom*).

The accuracy is at a level of a few percent for galaxies with high signal-to-noise, and worse for fainter galaxies.

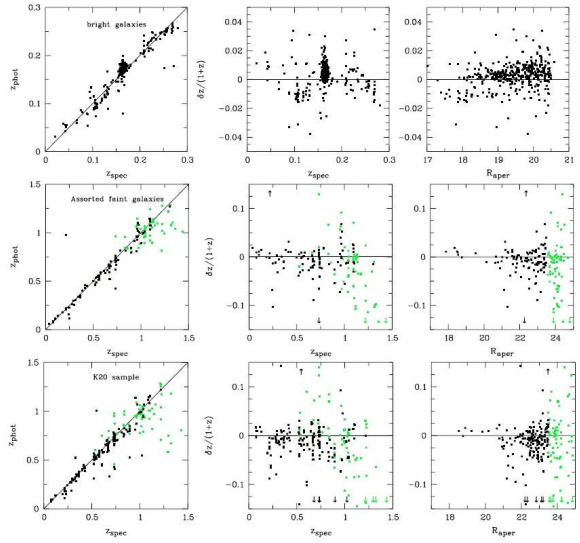

Fig. 17. Redshift quality of galaxies: *Top row*: 404 bright galaxies observed with 2dF, mostly containing galaxies from the supercluster field A901/902. *Left panel*: redshift comparison z_{phot} vs. z_{spec}. *Center panel*: redshift error $\delta z/(1+z)$ vs. redshift z_{spec}. *Right panel*: redshift error $\delta z/(1+z)$ vs. aperture R-band magnitude. The 1-sigma redshift error is <0.01, and the outlier rate for errors above 0.05 is <1% (3 out of 404 objects with errors around 0.06). *Center row*: a sample of 162 faint galaxies. Objects fainter than $R = 23.5$ are shown in grey. *Bottom row*: 247 galaxies from the K20 survey. Arrows in center or right column panels represent outliers with more than 15% redshift error in $(1+z)$.

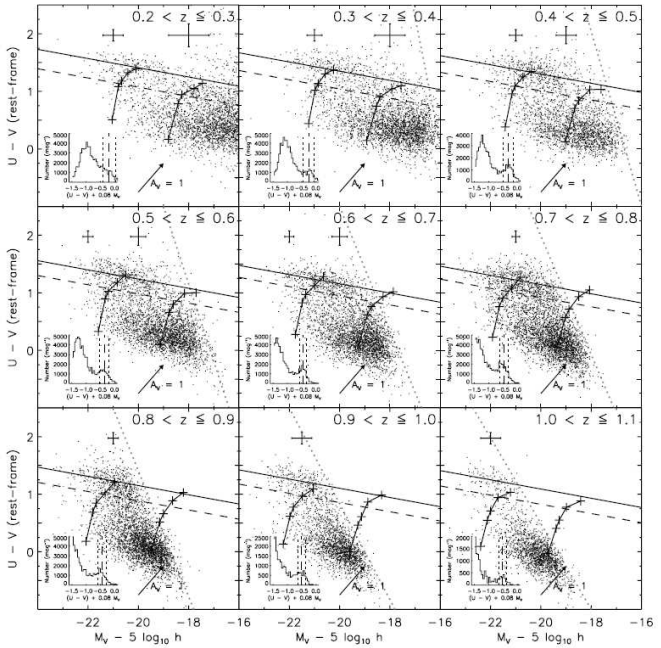

FIG. 1.—Rest-frame $U-V$ color of ~25,000 galaxies against the absolute magnitude in V band, $M_V - 5 \log h$. We show the distribution of galaxies in nine different redshift bins. A fit to the color-magnitude relation of red-sequence galaxies with a fixed slope of −0.08 is shown by the solid line, and the Butcher-Oemler–style cut between red and blue galaxies is shown by the dashed line parallel to the early-type galaxy CMR (see § 5). The sloping cutoff in the distribution of galaxies at the faint end is due to the $m_R \leq 24$ mag limit of the survey. This cutoff cannot be exactly depicted because of the color dependence in completeness and the varying transformation between observed R-band magnitude and rest-frame V-band magnitude; nevertheless, the dotted gray line shows very schematically the rough completeness limit. The lines with crosses show the colors and magnitudes of model galaxies with truncated SFHs at constant stellar mass, described in more detail in § 6.4. Representative error bars are shown. For reference, we show a reddening vector from Calzetti et al. (2000), assuming $A_V = 1$ mag; a Milky Way extinction curve gives the same vector. Shown in the insets is the color distribution of the red peak at each redshift (with the slope of the CMR taken out); the dashed line indicates the position of the biweight mean that we adopt as the CMR ridgeline, and the dotted lines show the biweight σ that we adopt as the CMR red sequence's scatter.

The resulting color magnitude diagram looks like this. Very good !

The interesting thing is that the red sequence looks just as prominent in the COMBO-17 data as in the DEEP 2 data. Notice that COMBO-17 has more galaxies - 25.000.

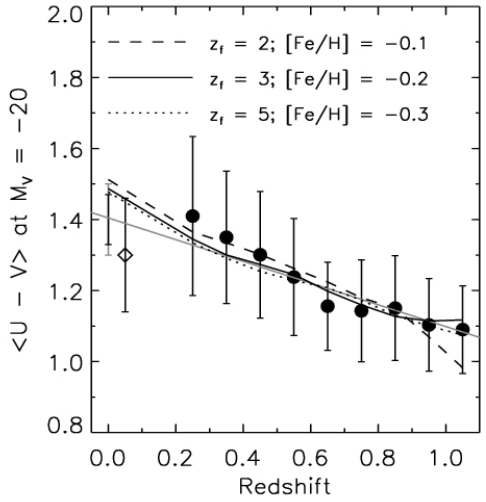

FIG. 2.—Color evolution of the red sequence, represented by the intercept of the CMR fits at $M_V - 5\log h = -20$ (*circles*) as a function of redshift. The error bars show the biweight scatter in each redshift bin. These highly conservative errors are much larger than the formal errors and likely overestimate the systematic errors from calibration, template/galaxy SED mismatches, and small redshift focusing issues, which we expect to be less than 0.1 mag in $U-V$ color. The lines show the expected color evolution of single-age stellar populations with different formation redshifts and metallicities, as given in the label. The diamond with error bars (offset from zero redshift for clarity) shows the $U-V$ CMR zero point at $z = 0$ synthesized from SDSS *ugr* data analyzed in the same way as these data (see the Appendix for details). The naked error bars show the $U-V$ CMR zero point for the A754 galaxy cluster (McIntosh et al. 2004), which is also consistent with the Nearby Field Galaxy Survey (Jansen et al. 2000) early-type galaxy CMR. The black naked error bar shows the A754 scatter around the CMR, and the expected systematic uncertainty is shown by a gray error bar. The gray line shows a fit to all the data (including the A754 and SDSS colors).

This figure shows how the colors of the galaxies evolve with redshift. The evolution one expects from the models depends in a simple way on the formation redshift. This is simply due to the fact that the color evolution is a simple power-law with time $color = constant * log(t)$. Hence, if the galaxies formed at higher redshift, they evolve slower. The slow evolution suggests that the galaxies formed early ($z > 2$?).

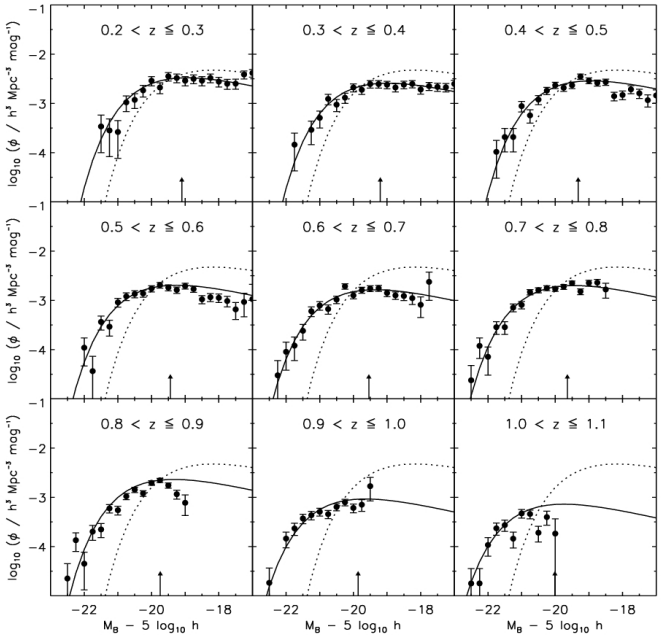

FIG. 3.—Redshift evolution in the rest-frame *B*-band luminosity function of red-sequence galaxies. Black solid lines with data points show the Schechter function fits and V/V_{max} luminosity functions of COMBO-17 red-sequence galaxies in each redshift interval. The dotted line shows the Schechter fit to the low-redshift SDSS comparison sample (see the Appendix for more details). A single faint-end slope $\alpha = -0.6$ is derived by a single STY fit to the COMBO-17 data at all redshifts. When deriving the ϕ^* estimate, the three least luminous bins are ignored. The arrow shows the magnitude cutoff used for the analysis of the luminous red-sequence galaxy population in § 6.4, assuming $z_f = 3$.

This figure shows the luminosity function of the red sequence at different redshifts. The luminosity functions are well determined out to $z = 0.8$.

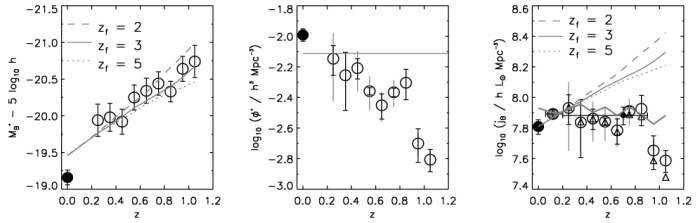

FIG. 4.—Evolution of the rest-frame B-band luminosity function of the red-sequence galaxy population from COMBO-17. *Left*: Evolution of M_B^*, the "knee" of the luminosity function. We show the expectations of a passive evolution model as smooth gray lines (with formation redshift shown in the figure legend). The solid point shows the M_B^* of the SDSS low-redshift comparison sample, transformed from u*g*r data (see the Appendix for more details). *Middle*: Evolution of ϕ^*. Again, open circles denote COMBO-17 data, and the solid point denotes the local SDSS sample. The error bars attempt to indicate uncertainty because of cosmic variance; the black error bars show the observed field-to-field variation divided by $\sqrt{3}$, whereas the gray error bars show the predicted cosmic variance by using the prescription of Somerville et al. (2004). A passive evolution model predicts no evolution in the number density with redshift (*gray line*). *Right*: Rest-frame B-band luminosity density per comoving Mpc^3 is shown by open circles, with error bars again denoting the uncertainties from cosmic variance. To reduce the cosmic variance uncertainty, we show also the averaged $0.2 \le z \le 0.9$ luminosity density j_B by the solid black circle, which has only a 13% uncertainty from cosmic variance. The upward pointing triangles denote a lower limit to the luminosity density, where only the observed luminosity density is accounted for (i.e., no extrapolation to zero luminosity). The filled gray point denotes the luminosity density of spectral type–selected early-type galaxies in the 2dFGRS. We show also the blind prediction of the Cole et al. (2000) semianalytic galaxy formation model as a solid gray curve, for which model galaxies were selected using exactly the same color cut methodology as used in this paper.

The characteristic brightness of galaxies increases with redshift(left), but the density goes down (middle), and the luminosity density (the integral of the luminosity function multiplied with the luminosity per galaxy) is constant. This is a real surprise.

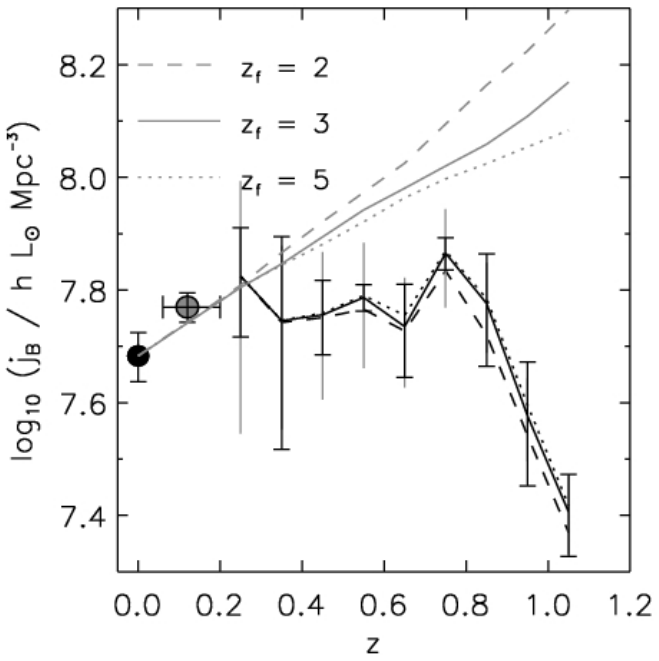

FIG. 5.—Luminosity density evolution of luminous red-sequence galaxies. The luminosity density of those red-sequence galaxies destined to evolve passively into galaxies brighter than $M_B - 5\log h \le -19.1$ at $\langle z \rangle = 0.25$ is shown by dashed, solid, and dotted black lines for $z_f = 2$, 3, and 5, respectively. The smooth gray curves show the expected evolution of a galaxy population that completely formed at high redshift and simply aged to the present day. The error bars show uncertainties from cosmic variance.

The luminosity density is nearly flat, but models predict that it should rise. The models assume that galaxies remain on the red sequence since $z = 2$. Those galaxies are much younger by $z = 1$ compared to $z = 0$, and hence should be brighter. Why not ? This is the question. Bell speculated that this is due to merging.

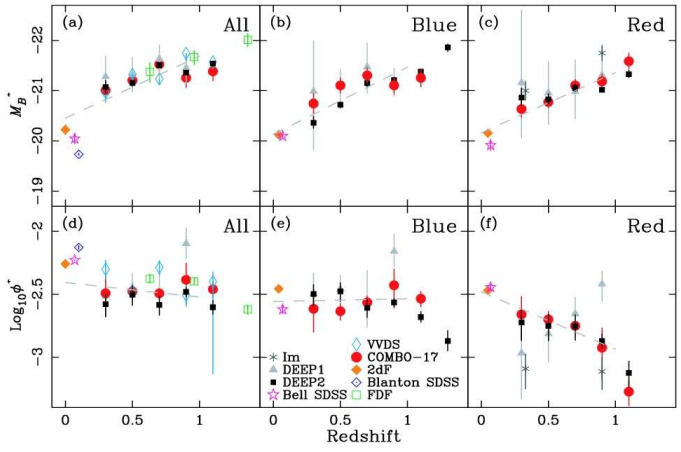

FIG. 7.—Evolution with redshift of the Schechter function parameters M_B^* (*top row*) and ϕ^* (*bottom row*) for the All, Blue, and Red galaxy samples. Data values for DEEP2 and COMBO-17 come from Tables 2–4. These parameters were calculated keeping the faint-end slope parameter α fixed to the "quasi-local" COMBO-17 values (−1.3 [All], −1.3 [Blue], and −0.5 [Red]). Error bars on DEEP2 and COMBO-17 are Poisson 68% values for M_B^* and Poisson errors convolved in quadrature with cosmic variance for ϕ^* (see text). Also shown are the Schechter parameters from the other works summarized in Table 5. Estimates for distant galaxies come from Ilbert et al. (2005, VVDS, panels [*a*] and [*d*]) and Gabasch et al. (2004, FDF, panels [*a*] and [*d*]). Previous DEEP1 values from Im et al. (2002) are discussed in the text. Local values come from Bell et al. (2003) and Blanton et al. (2003) using SDSS and from Norberg et al. (2002) and Madgwick et al. (2003) using 2dF. The dashed gray lines represent linear fits vs. z to the evolution of M_B^* and ϕ^* shown in Table 6; the data fitted are the local surveys plus COMBO-17 and DEEP2 (out to $z = 1$). M_B^* brightens by ∼1.2–1.3 mag at $z = 1$ for all colors, but galaxy number density (ϕ^*) differs markedly with color: Blue number densities remain roughly constant after $z = 1$, Red number densities rise with time, while the All sample is a blend of the two.

Faber et al. combined the results of Bell et al. with the DEEP 2 results. They split the galaxies into blue and red galaxies.

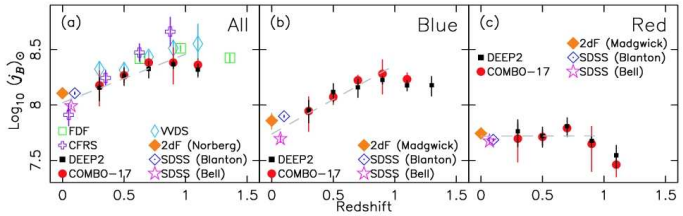

FIG. 8.—Evolution of the comoving *B*-band luminosity density in units of solar luminosities per Mpc^3, vs. redshift. Data values for COMBO-17 and DEEP2 come from Tables 2–4. References and symbols are the same as in Fig. 7 except for CFRS (*blue crosses*), which comes from Lilly et al. (1996). The blue and red estimates from Blanton et al. (2003) use the total luminosity density from that paper corrected by a contribution due to red galaxies of 38% from Hogg et al. (2002; see text). The dashed gray lines are as in Fig. 7 and show the linear fits to z from Table 6; data used include the local surveys plus COMBO-17 and DEEP2 (out to $z = 1$). The luminosity density of blue galaxies has decreased by about a factor of 4.2 since $z = 1$, while that for red galaxies has remained roughly constant, with a possible rise before that.

The luminosity density of the red galaxies is constant, and that of the blue galaxies is evolving. It is going down from high redshift to low redshift.

This result is consistent with the Bell et al result. So what happens ?

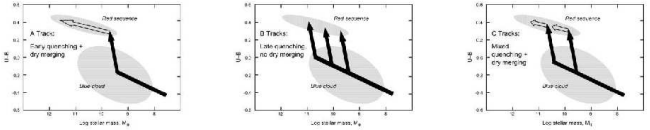

FIG. 10.—Schematic arrows showing galaxies migrating to the red sequence under different versions of the merging hypothesis. Evolutionary tracks are plotted in the color-mass diagram. Here it is assumed that red galaxies arise from blue galaxies when star formation is quenched during a major merger, causing the galaxy to double in mass, but the exact nature of the quenching mechanism is not crucial. Quenching tracks are shown by the nearly vertical black arrows. The mergers would be gas-rich (or "wet") because the progenitor galaxies are blue objects making stars and hence contain gas. Once a galaxy arrives on the red sequence, it may evolve more slowly along it through a series of gas-poor, or "dry," mergers. These are shown as the white arrows. They are tilted upward to reflect the aging of the stellar populations during the more gradual dry merging. A major variable is the time of mass assembly vs. the time of quenching. Three possibilities are shown. Track A represents very early quenching while the fragments of the galaxy are still small. In that case, most mass assembly occurs in dry mergers along the red sequence. Track B is the other extreme, having maximally late quenching. In that case, galaxies assemble most of their mass while still blue and then merge once to become red with no further dry merging. Track C is intermediate, with contributions from both mechanisms. This "mixed" scenario best matches the properties of both distant and local ellipticals. In addition to the merging scenario illustrated here, the gas supply of some disks may simply be choked off or stripped out without mergers, to produce disky S0s. Such tracks would be vertical, but aside from this their histories are similar. S0s dominate on the red sequence below L^*, ellipticals above (Marinoni et al. 1999).

Faber et al. (and in a different paper, Bell et al.) suggest various explanations. One is merging, the other is that blue galaxies stop forming stars at some stage, become red (move up), and then merge (move left). Probably all those processes play a role.
All in all, the results are intruiging, if true: we expect that the luminosity density of the red galaxies goes down with time - but instead, it remains constant; and we expect the luminosity density of blue galaxies to remain constant with time (or to increase); and instead it decreases !

Measuring masses

One of the issues with the results above is that it is all based on measurements of light. Models are used to transform those measurements into estimates of stellar mass. The questions is, are those models correct ?

For early-type galaxies, we can check directly. We can simply measure the motions of the stars, by measuring the velocity dispersions. With long integration times, we can now do this to high redshift (Franx 1993, van Dokkum et al 1996, 1998, vd Wel et al 2003). An example is shown below:

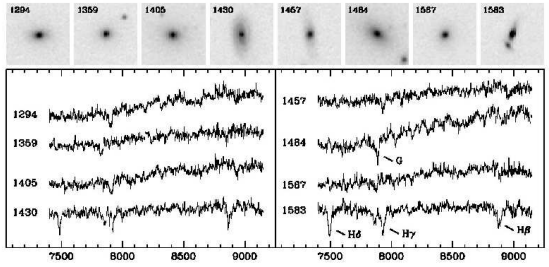

FIG. 1.—*HST* images and Keck spectra of the galaxies in MS 1054−03 with measured dispersions. The most prominent spectral feature in most galaxies is the 4300 Å *G* band observed at ≈7870 Å. Galaxies 1430 and 1583 have strong Balmer absorption lines and are "*E* + *A*" galaxies. Galaxy 1484 is the brightest cluster galaxy.

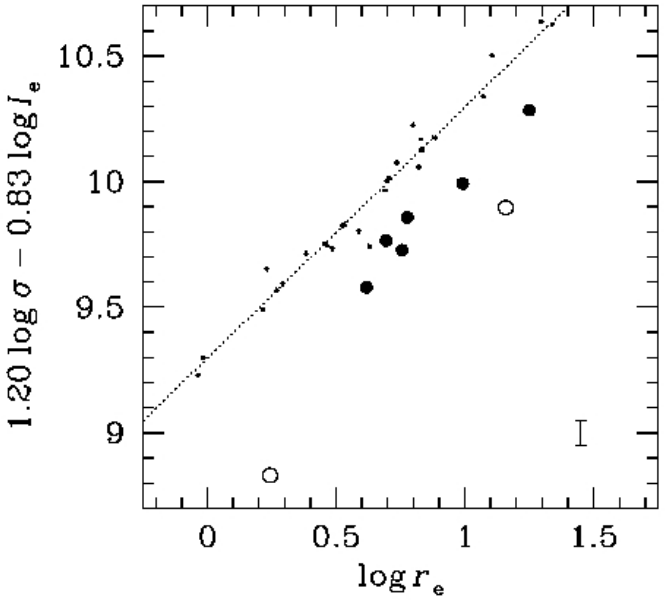

FIG. 2.—Edge-on projection of the fundamental plane in MS 1054−03 at $z = 0.83$. The open circles are two $E + A$ galaxies. The error bar indicates the typical uncertainty. The small dots are galaxies in Coma at $z = 0.023$, from JFK. The line shows the fit from JFK. The fundamental plane for the six galaxies with early-type spectra is very similar to the FP of Coma. The offset with respect to the FP of Coma is due to the luminosity evolution of the galaxies.

This is the Fundamental Plane that is derived from this. The small scatter is remarkable. This allows an accurate measurement

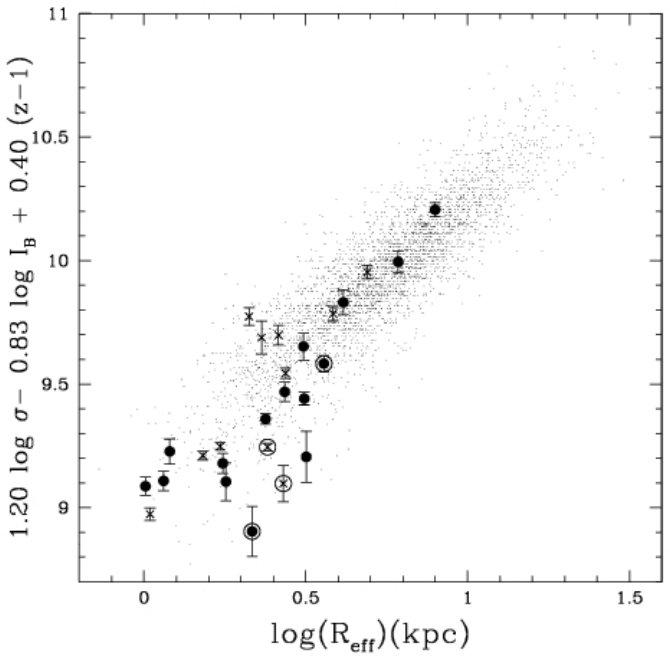

FIG. 5.—FP of our sample of early-type galaxies compared to the field early-type galaxy sample from SDSS (*small filled circles*; Bernardi et al. 2003). The objects in the primary sample, early-type galaxies at $z \sim 1$ that satisfy all of our selection criteria, are indicated by the large filled circles. The crosses are fillers, mainly galaxies at redshifts $z \sim 0.7$. Encircled objects have one or more emission lines in their spectra. The surface brightness, I_B, of every galaxy in this figure is corrected for evolution to a value it would have at $z = 1$, assuming $\Delta \ln (M/L_B) = -1.12\,z$, which is the evolution of massive cluster galaxies. The FP already existed at $z = 1$ for a large range in size.

Van der Wel et al extended the results to the field. These studies are harder: in clusters, it is easy to observe many galaxies at the same time. In the field, this is harder - it takes more telescope time to observe the same number of galaxies .

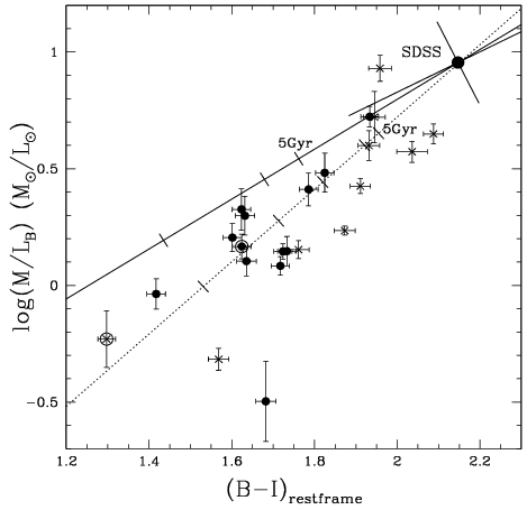

FIG. 7.—Rest-frame $B - I$ color vs. M/L_B for our early-type galaxy sample. For an explanation of the symbols, see Fig. 6*a*. The large filled circle at the upper right indicates the median $B - I$ and M/L_B of the massive galaxies ($M > 2 \times 10^{11}\ M_\odot$) in the SDSS field early-type galaxy sample. The orientation of the distribution around the median values and the amount of scatter are indicated by the tilted error bars. The dotted line is a solar metallicity Bruzual-Charlot model for a single stellar population. The solid line is a model with exponentially declining star formation ($\tau = 1$ Gyr). Both model tracks are shifted vertically to match the SDSS data point. Model ages are indicated by ticks at intervals of 1 Gyr. The correlation between M/L and color implies that the observed scatter in M/L is real and can be ascribed to age differences between the stellar populations of the galaxies. Our $i - z \geq 0.86$ color selection limit roughly corresponds to $B - I \geq 1.1$ according to the Bruzual-Charlot models. This shows that our selection criterion only excludes galaxies with ages less than 1 Gyr and does not affect our conclusions regarding the massive, red galaxies. [*See the electronic edition of the Journal for a color version of this figure.*]

The mass-to-light ratio correlates nicely with color

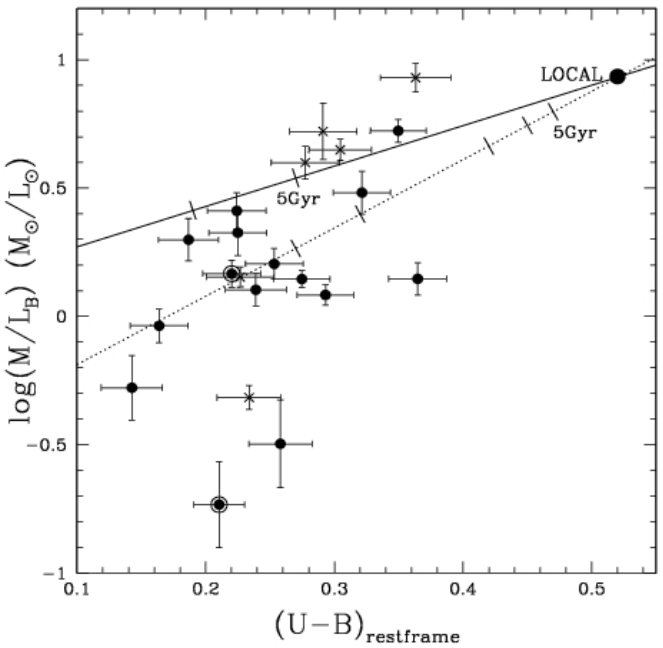

FIG. 8.—Rest-frame $U-B$ color vs. M/L_B for the early-type galaxy sample. For an explanation of the symbols, see Fig. 6*a*. The "LOCAL" data point is taken from G03. There is a similar relation as in Fig. 7, but it is less clear because the range of colors is much smaller in $U-B$ than in $B-I$. Our $i-z \geq 0.86$ color criterion corresponds to $U-B \geq 0.07$ at $z=1$, which demonstrates that this criterion would only exclude the most extremely blue galaxies (with ages well below 1 Gyr). [*See the electronic edition of the Journal for a color version of this figure*.]

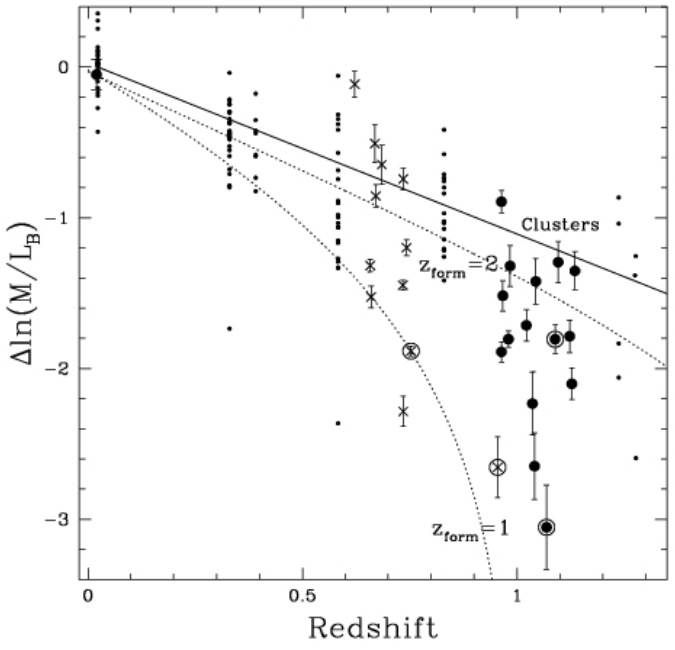

FIG. 6.—Offset from the local FP in the rest-frame B band for individual cluster galaxies taken from the literature (*small filled circles*) and the early-type galaxies with high-S/N spectra in our sample. We distinguish, as in Fig. 5, between the primary sample (*large filled circles*) and the fillers (*crosses*). The cluster samples are taken from Jørgensen et al. (1996), Kelson et al. (2000), van Dokkum & Franx (1996), Wuyts et al. (2004), Holden et al. (2005), and van Dokkum & Stanford (2003). The solid line is $\Delta \ln (M/L_B) = 1.12z$, which is the best-fitting straight line for the evolution of cluster galaxies with masses $M > 2 \times 10^{11}\ M_{\odot}$. The dotted lines are model tracks for a single stellar population with formation redshifts 1 (*lower line*) and 2 (*upper line*; see text for a more detailed explanation). These model tracks are forced to go through the black filled circle at $z=0.02$, which represents the field galaxies in the sample of Faber et al. (1989). The range in offsets from the local field FP is large, but there is a strong correlation with mass. Massive field galaxies evolve as fast as equally massive cluster galaxies, while less massive galaxies evolve faster. [*See the electronic edition of the Journal for a color version of this figure*.]

This is the result. The massive field galaxies evolve as slowly as cluster galaxies. The lower mass field galaxies maybe not - but this can be a selection effect.
All in all, the result from the Fundamental Plane show that the mass-to-light ratios of early-type galaxies evolve quickly with redshift. Hence the fact that the luminosity density of early-types is constant translates directly into the conclusion that the mass density must decrease with increasing redshift